J. Fluid Mech. (2007), *vol.* 570, *pp.* 407–429.
doi:10.1017/S0022112006003296 Printed in the United Kingdom

On the boundary integral method for the rebounding bubble

By M. LEE[1,2], E. KLASEBOER[3] AND B. C. KHOO[2,4]

[1]Department of Mechanical Engineering, Sejong University, Seoul, 143-747 Korea
[2]Department of Mechanical Engineering, National University of Singapore, 10 Kent Ridge Crescent, Singapore 119260
[3]Institute of High Performance Computing, 1 Science Park Road #01-01 The Capricorn, Singapore 117528
[4]Singapore-MIT Alliance, 4 Engineering Drive 3, Singapore 117576
mlee@sejong.ac.kr, evert@ihpc.a-star.edu.sg, mpekbc@nus.edu.sg

(Received 2 February 2005 and in final form 8 June 2006)

The formation of a toroidal bubble towards the end of the bubble collapse stage in the neighbourhood of a solid boundary has been successfully studied using the boundary integral method. The further evolution (rebound) of the toroidal bubble is considered with the loss of system energy taken into account. The energy loss is incorporated into a mathematical model by a discontinuous jump in the potential energy at the minimum volume during the short collapse–rebound period accompanying wave emission. This implementation is first tested with the spherically oscillating bubble system using the theoretical Rayleigh–Plesset equation. Excellent agreement with experimental data for the bubble radius evolution up to three oscillation periods is obtained. Secondly, the incorporation of energy loss is tested with the motion of an oscillating bubble system in the neighbourhood of a rigid boundary, in an axisymmetric geometry, using a boundary integral method. Example calculations are presented to demonstrate the possibility of capturing the peculiar entity of a counterjet, which has been reported only in recent experimental studies.

1. Introduction

The dynamics of a non-equilibrium violently oscillating gas bubble have been studied extensively for many decades. The early works on bubble dynamics focused on underwater explosions (Taylor 1942; Cole 1948). Laser-generated cavitation was developed in the early 1970s for experiments with a single transient bubble (Lauterborn 1972). Some studies have also been undertaken in new areas such as medical ultrasonics and sonochemistry (Leighton 1994).

The motion of a spherically oscillating bubble system is described briefly below. Because of the initial high pressure in a small volume, the bubble starts to expand against the surrounding medium almost immediately. The expansion continues for a relatively long time, and the internal gas pressure decreases gradually. However, inertia causes the bubble to over expand and the pressure inside the bubble becomes lower than the surrounding reference pressure; it then stops expanding. The hydrostatic pressure is now considerably larger than the pressure inside the bubble ($\sim$0.1 bar) and then a collapse phase ensues. This contraction phase continues until the gas pressure becomes much larger than the surrounding fluid pressure and then a second

expansion follows. Finally, the bubble becomes an oscillating system owing to the inertia of the water together with the pressure of the gas. The bubble undergoes several cycles of expansion and contraction, each time with reduced amplitude owing to the loss of system energy. Experiments reveal that the total energy of the bubble at the second cycle is only around 30 % of that at the first cycle (Cole 1948; Buogo & Cannelli 2002).

The dynamics of transient bubbles adjacent to a rigid boundary are of great interest to engineers because of the potential destructive action of bubbles on solid surfaces. One of the distinguished phenomena is the evolution of a toroidal bubble. The asymmetry is introduced into the flow field because of the presence of the rigid boundary, so that the bubble evolves into a toroidal form during collapse (Benjamin & Ellis 1966). This was demonstrated well both numerically and experimentally by Tomita & Shima (1986).

The boundary integral method is well developed for use in calculating the evolution of bubbles with the assumption of an ideal fluid flow that is inviscid and irrotational (Blake, Taib & Doherty 1986; Chahine & Perdue 1988; Boulton-Stone 1993; Pearson, Blake & Otto 2004). This method was extended to the analysis of a toroidal bubble (doubly connected geometry) by introducing a dynamic cut in the flow domain, which allows the bubble to be considered as singly connected (Best & Kucera 1992). Since the potential function in a doubly connected flow field is non-unique, another approach using a vortex ring inside the bubble was introduced by Lundgren & Mansour (1991) and also adopted in Wang *et al.* (1996) for simulating the transition of the original singly connected bubble into the toroidal bubble.

However, most of the previous computations using the boundary integral method have been applied only up to about the first collapse (one cycle), since the analyses did not take into account the system energy loss (Brujan *et al.* 2002). In fact, during the bubble's life, undergoing several oscillations, a series of energy deposition mechanisms would be involved with significant loss mechanisms; there are kinetic and potential energies of the bubble and the liquid, potential energy due to buoyancy, and potential energy due to surface tension. Some of the loss mechanisms are due to pressure pulse radiation into the liquid, chemical reactions, molecular relaxation in the gas, heat and mass transfer at the bubble surface. Some of these could be primary, some are secondary, and some are negligible (Geers & Hunter 2002). The emission of bubble pulses that could be the main loss mechanism is significant only in a small interval about the time of minimum volume. The bubble pulse builds up to a maximum value at minimum volume and falls off again as the bubble expands. The phenomena of collapse and rebound accompanying shock-wave emission of a single laser-generated cavitation bubble were investigated experimentally by means of high-speed cinematography by Lindau & Lauterborn (2003). They observed two compression shock waves (*jet torus shock wave* and *tip bubble shock wave*) emitted in rapid succession when the bubble reaches minimum size and maximum compression.

An early calculation for the rebound of a non-spherical bubble and possibly the rejoining into a singly connected bubble, which is the next stage of the toroidal bubble development, was demonstrated numerically with no consideration of energy loss (Best 1994). In the current work, we aim to produce a more realistic result for the oscillating bubble system undergoing more than one cycle. The loss of system energy is employed with a discontinuous jump condition (as a fraction of total system energy) in the potential energy (via bubble pressure) at the minimum volume during the short collapse–rebound period. The energy loss mechanisms due to compressibility, viscosity and radiation involve further complex physics (Putterman & Weninger 2000), and

the magnitude of their contributions is expected to vary in different physical regimes. This is beyond the scope of the present work.

To demonstrate this implementation, we first examine a spherically oscillating bubble system up to two or three cycles in terms of the maximum bubble radii, bubble periods and fractions of energy lost in each cycle. The theoretical Rayleigh–Plesset equation with the loss of system energy taken into account is found to match well with available experimental data. With the promising result for the spherical bubble system, the analysis of axisymmetric flow configurations using the boundary integral method has been conducted with the same implementation of the energy loss model. One of the challenges for the computation of a bubble near a wall is the counterjet that has only been reported in experiments (Tomita & Shima 1986; Vogel, Lauterborn & Timm 1989; Ward & Emmony 1991; Philipp & Lauterborn 1998; Kodama & Tomita 2000; Lindau & Lauterborn 2003). Since the counterjet develops during the rebound (beginning of second cycle), the boundary integral formulation must take into account the loss of system energy.

2. Theory

We describe the fluid as inviscid and incompressible and the flow induced by the bubble's motion as irrotational. Hence, the velocity field u can also be described using potential theory, and the velocity potential satisfies the Laplace equation

$$u = \nabla\phi \quad \text{where } \nabla^2\phi = 0. \tag{2.1}$$

At the bubble surface, if no surface-tension effects are taken into account, the pressure in the fluid must be continuous and equal to the pressure inside the bubble P_b. This pressure is assumed to be uniform inside the bubble and consists of two parts: one part resulting from the gas content of the bubble and one part vapour. It is assumed that the gas inside the bubble behaves as an ideal gas and there is negligible heat exchange with the surrounding fluid, so that the expansion and compression of the gas content of the bubble are adiabatic. The vapour pressure P_v is a function of the temperature of the bubble wall only and is assumed to be small for most cases under investigation ($P_v \sim 2$ kPa at 20 °C) and is often neglected (Klaseboer *et al.* 2005) since it is usually much smaller than the atmospheric or reference pressure of the system. However, it might become important under certain circumstances such as in spark-generated bubbles of maximum radius 35 mm as used by Buogo & Cannelli (2002), where the vapour pressure was about $P_v = 0.3$ bar for the first oscillation cycle of the bubble and 0.06 bar for the second cycle, indicating the heating up of the bubble wall and its subsequent cooling down for the second cycle (the values 0.3 bar and 0.06 bar correspond to wall bubble wall temperatures of 69 and 36 °C, respectively). Similar results were found by Lew, Klaseboer & Khoo (2006) where an even larger value of $P_v = 0.4$ bar was measured for the first cycle for spark-generated bubbles with maximum radii of 3 to 5 mm. Dalton's law for mixtures of ideal gases states that the pressures of the vapour and the gas can be added. Hence, the bubble pressure as a function of the volume, V, is described as (Best & Kucera 1992; Brennen 1995)

$$P_b = P_v + P_{g,0}\left(\frac{V_0}{V}\right)^{\lambda}, \tag{2.2}$$

where the subscript 0 denotes initial quantities, λ is the ratio of the specific heats for the gas and empirically determined. The term $P_{g,0}$ is the pressure at the initial state and is usually of the order of magnitude of 100 to 500 bar. The equation for the

vapour pressure inside implicitly assumes that the vapour evaporates when the bubble expands and condensation occurs at the bubble surface when the bubble shrinks. This will keep the vapour pressure at a constant value. This is only valid when the speed of the bubble wall is small compared to the speed of sound (or the Mach number $\ll 1$). In most practical cases, the speed of the bubble wall will not exceed $100\,\mathrm{m\,s^{-1}}$ and thus this condition is satisfied. The mass of the gas inside the bubble is assumed to be constant, since diffusion into the liquid is minimal during the time scales we are looking at. Also, it is implicitly assumed that the vapour and gas are diluted enough so they do not influence each other (Dalton's law). We will focus on an oscillating system undergoing more than one cycle, in which some of the energy in the bubble system is lost at each cycle, so we expect progressively decreasing maximum bubble radii and periods.

2.1. *Energies in the oscillating bubble system*

We shall describe the total energy E in the oscillating system. Note that the total mechanical energy is conserved only within one cycle. It consists of the work done by the bubble (potential energy, E_p) and the kinetic energy E_k (Cole 1948; Pearson *et al.* 2004)

$$E = -\int_{V_0}^{V} P_{g,0}(V_0/V)^{\lambda}\,\mathrm{d}V + \int_{V_0}^{V} \Delta P\,\mathrm{d}V + \tfrac{1}{2}\rho\int_{\Omega} u^2\,\mathrm{d}\Omega = \text{constant for each cycle}, \tag{2.3}$$

with $\Delta P = P_\infty - P_v$ and $P_\infty = P_{ATM} + \rho g h$ the reference pressure at the hydrostatic depth h far away from the bubble, where P_{ATM} is the atmospheric pressure (1 bar), g the acceleration due to gravity and ρ is the fluid density. The potential energy E_p consists of two terms (the first two integrals in (2.3)); the first integral results from the energy added to the system due to the bubble pressure and the second integral originates from the fact that some work is done at infinity due to the conservation of volume in the fluid corrected by a term due to the vapour pressure (Cole 1948). The total kinetic energy E_k of the system is obtained by taking the square of the absolute velocity u, multiplying it by the fluid density (i.e. the kinetic energy per unit mass) and integrating it over the whole fluid domain Ω (third integral in (2.3)). The bubble will reach each maximum bubble radius, $R_{m,n}$ for the nth oscillation with oscillation period T_n.

Non-dimensionalization of the equations is now employed with scaling parameter for all lengths the first maximum bubble radius $R_{m,1}$, for volumes with $R_{m,1}^3$, for all pressures with ΔP, for velocities with $\sqrt{\Delta P/\rho}$, for potentials with $R_{m,1}\sqrt{\Delta P/\rho}$ and finally for time with $R_{m,1}\sqrt{\rho/\Delta P}$. From now onwards, all variables with an overbar are considered as dimensionless. With the help of the Gauss theorem, equation (2.3) can be rewritten as an integral over the surface of the bubble only. The final non-dimensional equation is simply given by (Wang & Khoo 2004)

$$\left[\frac{\varepsilon_n}{\lambda-1}\left(\frac{\bar{V}_0}{\bar{V}}\right)^{\lambda}+1\right]\bar{V} + \tfrac{1}{2}\int_S \bar{\phi}\frac{\partial\bar{\phi}}{\partial n}\,\mathrm{d}\bar{S} = \frac{\varepsilon_n}{\lambda-1}\bar{V}_0 + \bar{V}_0. \tag{2.4}$$

Here, the subscript '0' corresponds to the time when the new cycle starts. Buoyancy effects are neglected, but could easily be included by adding a term $\delta^2\bar{z}_c\bar{V}$ to the left-hand side of (2.4), where z_c is the depth of the bubble centre and $\delta = \sqrt{\rho g R_m/\Delta P}$ is the so-called buoyancy parameter (Best 1993). This is justified when the maximum bubble radius is small (several mm) or the reference pressure is relatively large. For underwater explosions, where the bubble radius can reach up to many metres, the

gravity term must be included. In (2.4), a term with the normal velocity on the bubble surface appears which is defined as $\partial\phi/\partial n = \boldsymbol{n}\cdot\nabla\phi$. For any fixed solid structure (if present), this normal velocity is zero (no penetration of the fluid into the solid) and will thus give a zero contribution to the kinetic energy. The strength parameter for the nth oscillation is defined as $\varepsilon_n = P_{g,0}/\Delta P$, which provides some measure of the magnitude of the initial pressure exerted by the bubble contents.

In reality, the second period of the bubble becomes less violent. It is therefore necessary to incorporate the loss of energy into the system. The violent bubble behaviour associates the emission of energy in the form of pressure pulses propagating radially outward from the bubble. Other possible mechanisms for energy dissipations during bubble collapse are thought of as turbulent flow dissipating energy in the form of eddies owing to mean convective velocity of the bubble, thermal conduction through the bubble, energy loss due to jet impacts and liquid compressibility. A detailed examination of each of these mechanisms is beyond the scope of this work.

The loss of energy is most likely to occur in the vicinity of each minimum volume. We can neglect the short period of emission of energy compared to the length of the total bubble period owing to the very rapid event of the emission process (see also Buogo & Cannelli 2002; Delale & Tunç 2004). Consequently, the loss of energy is assumed to take place instantaneously at the bubble minimum volume with a discontinuity in the potential energy from the available energy to a lower energy state corresponding to the fraction of available energy remaining; this is to be provided from experimental data. That is, at each minimum volume, the strength parameter is discontinuously replaced by a new value ε_n, to drop the potential energy into a next energy level discontinuously such that (using (2.4))

$$\frac{E_{n+1}}{E_n} \approx \frac{\varepsilon_{n+1}}{\varepsilon_n} < 1. \tag{2.5}$$

Here, E_n is the fraction of energy which remains for the nth oscillation of period T_n.

As a relatively simple approach, the bubble energy in each cycle can be estimated experimentally by measuring the bubble potential energy from its maximum size (Buogo & Cannelli 2002)

$$\frac{E_{n+1}}{E_n} = \left(\frac{R_{m,n+1}}{R_{m,n}}\right)^3 \left(\frac{P_\infty - P_{v,n+1}}{P_\infty - P_{v,n}}\right). \tag{2.6}$$

There is also a useful correlation for the bubble period which varies as the cube root of the total energy and the negative 5/6 power of the hydrostatic pressure (Cole 1948)

$$\frac{E_{n+1}}{E_n} = \left(\frac{T_{n+1}}{T_n}\right)^3 \left(\frac{P_\infty - P_{v,n+1}}{P_\infty - P_{v,n}}\right)^{5/2}. \tag{2.7}$$

This correlation permits an estimate of energy loss in successive contractions from the easily obtained ratio of periods.

Another often used correlation is Rayleigh's (1917) formula which relates R_m to the collapse time t_c (or half-time between the two minimum volumes; $t_c = T_n/2$) for each cycle via

$$\frac{R_m}{t_c} = 1.09\sqrt{\frac{P_\infty - P_v}{\rho}}. \tag{2.8}$$

Finally it is emphasized that the above three correlations should be consistent, and can be further employed for the evaluation of the results.

2.2. *Bubble pulse*

The assumption of incompressible fluid leads to a fairly accurate description of the main features of gas bubble dynamics, particularly of the maximum radius and the period of pulsation. One of the important phenomena associated with an oscillating bubble system is the emission of bubble pulses, which is the main mechanism of energy loss from the system. The pressure pulse is analogous to the spherical/cylindrical implosion problem where as the contact discontinuity (interface) is undergoing contraction symmetrically, a shock is generated and propagated radially inwards towards the centre to be reflected and subsequently radiated outwards. All the above happens in a very short time where the interface hardly moves while a significant portion of the overall energy of the system associated with the outward radiating shock is convected away.

Lindau & Lauterborn (2003) observed, in a laser-induced cavitation bubble in liquid, the presence of shock wave(s) at about the bubble minimum volume although no quantitative measurement is made of the shock energy convected away. Cole (1948) has suggested, '... the mechanism by which energy can be dissipated: the compressibility of the water, by which energy is radiated as a wave and ultimately dissipated in heat as the wave passes to infinite distance, and turbulent flow around...'. The first mechanism due to compressibility of the fluid is similar if not related to the implosion problem discussed above. On the second mechanism, Cole argued that '...a turbulent wake is formed as a result of water breaking away from the bubble surfaces,...forming eddies in which energy is dissipated by work done against viscosity...'. The rate of energy dissipation through viscous action taken to be proportional to the cube of mean bubble convective velocity (also shown experimentally by Taylor & Davies (1944) for air bubbles with deliberate convective rise velocity as released in various liquids) can therefore be deemed to be negligible, especially for the present stand-alone oscillating bubble with minimal mean motion. The largest movement of maximum convective velocity usually occurs at the bubble minimum volume. Lastly, Cole remarked that the other possible 'energy loss by direct thermal conduction for the short times and small temperature gradients is readily shown to be negligible, even in the gas sphere, if there is no turbulence.'

Most of the theory for the calculation of the bubble pulses in water is also based on the incompressible fluid flow descriptions. The pressure at any point in an incompressible liquid can be calculated from Bernoulli's equation in dimensionless form as

$$\bar{P} = 1 - \frac{\partial \bar{\phi}}{\partial \bar{t}} - \tfrac{1}{2}\bar{u}^2. \tag{2.9}$$

From the mass conservation of the bubble at two different radii, $\bar{u} = \dot{\bar{R}}\,\bar{R}^2/\bar{r}^2$ with the overdot denoting differentiation with respect to time. Here, R is the radius. With the potential, $\bar{\phi} = -\dot{\bar{R}}\bar{R}^2/\bar{r}$, (2.9) can be rewritten as

$$\bar{P} = 1 + 2\frac{\bar{R}}{\bar{r}}\left(\frac{\mathrm{d}\bar{R}}{\mathrm{d}\bar{t}}\right)^2 + \frac{\bar{R}^2}{\bar{r}}\frac{\mathrm{d}^2\bar{R}}{\mathrm{d}\bar{t}^2} - \frac{1}{2}\frac{\bar{R}^4}{\bar{r}^4}\left(\frac{\mathrm{d}\bar{R}}{\mathrm{d}\bar{t}}\right)^2. \tag{2.10}$$

In the following section we will apply (2.10) to the one-dimensional (spherical) bubble system. Once the result (such as bubble radius *vs.* time) is obtained from the Rayleigh–Plesset equation with incorporation of the energy loss, (2.10) is used to predict the evolution of the successive bubble collapse pulses with diminishing magnitude.

3. Spherically oscillating bubble system

First, we consider a bubble oscillating in an infinite fluid with no gravity. The problem is spherically symmetric. By applying this boundary condition to the Bernoulli equation, we obtain the simplest form of the Rayleigh–Plesset equation (Brennen 1995)

$$\frac{P_b - P_\infty}{\rho} = \tfrac{3}{2}(\dot{R})^2 + R\ddot{R}, \tag{3.1}$$

The Rayleigh–Plesset equation can be rewritten in dimensionless form (Best & Kucera 1992) as

$$\bar{P}_g - 1 = \varepsilon_n \left(\frac{\bar{V}_0}{\bar{V}}\right)^{\lambda} - 1 = \frac{3}{2}\left(\frac{\mathrm{d}\bar{R}}{\mathrm{d}\bar{t}}\right)^2 + \bar{R}\frac{\mathrm{d}^2\bar{R}}{\mathrm{d}\bar{t}^2}. \tag{3.2}$$

This can be solved accurately by a standard ODE solver such as the fourth-order Runge–Kutta method. The bubble is initially supposed to be spherical and of radius $\bar{R}_0$ ($\bar{R}_0$ relates to the corresponding value $\bar{V}_0$ of (3.2)), and zero bubble wall velocity. For bubble explosion, $\lambda = 1.25$ as in Cole (1948). The three dimensionless parameters $\bar{R}_0$, λ and ε_1 cannot be chosen independently, but are correlated by an equation, which is deduced from the Rayleigh–Plesset equation (Klaseboer *et al.* 2005)

$$\frac{\varepsilon_1}{\lambda - 1}\left(\bar{R}_0^{3\lambda} - \bar{R}_0^3\right) = -1 + \bar{R}_0^3. \tag{3.3}$$

3.1. *Explosion bubble*

Consider the explosion of a 0.249 kg tetryl charge placed at a depth of $h = 91.44$ m below the surface. To compare with experimental data, dimensional parameters must be used in this case. An equation to calculate the first maximum bubble radius with charge weight W (in kg, TNT equivalent) and depth h is given in Cole (1948)

$$R_{m,1} = K_1 \left(\frac{W}{h + 10}\right)^{1/3}. \tag{3.4}$$

The bubble period–depth relation is found with an empirical constant K_2 (Cole 1948)

$$T_1 = K_2 \frac{W^{1/3}}{(h + 10)^{5/6}}, \tag{3.5}$$

where T_1 is the bubble period. The above equations are converted to SI units.

If the vapour pressures in (2.6) and (2.7) are assumed to be negligible (for most of the explosion bubble studies), a useful correlation for the bubble period and maximum radius which varies as the cube root of the total energy is obtained as

$$\frac{E_{n+1}}{E_n} = \left(\frac{T_{n+1}}{T_n}\right)^3 = \left(\frac{R_{m,n+1}}{R_{m,n}}\right)^3. \tag{3.6}$$

Table 1 gives the experimental data for the maximum bubble radii and bubble periods in terms of the total energy of the system. The data correlate well with (3.6). In general, the second bubble period and the bubble maximum radius are around 70 % of the first ones.

The parameters for the calculation of this example are: $\varepsilon_1 = 103.36$ and $\lambda = 1.25$ ($\bar{R}_0$ is calculated with (3.3) and is about 0.1467). Figure 1 shows the normalized energy variations for up to 3 cycles considered. The total mechanical energy of the system $E = E_k + E_p$ is assumed to be conserved during each cycle (Wang & Khoo 2004), since it reckoned that energy loss occurred primarily at the minimum volume (see

Cycle	First period	Second period	Third period
Fraction of available energy remaining (%)	100	34	54
Fraction of original energy remaining (%)	100	34	18
R_m (cm)	45.2	30.5	23.9
T (ms)	28.6	21.0	N/A

TABLE 1. Energy losses in contractions of the explosion-generated bubble, maximum bubble radii, and bubble periods for 0.249 kg TNT equivalent charge at 91.44 m depth from Cole (1948). $R_{m,2}/R_{m,1}$ (= 0.67) $\approx T_2/T_1$ (= 0.73) $\approx (E_2/E_1)^{1/3}$(= 0.70) using (3.6).

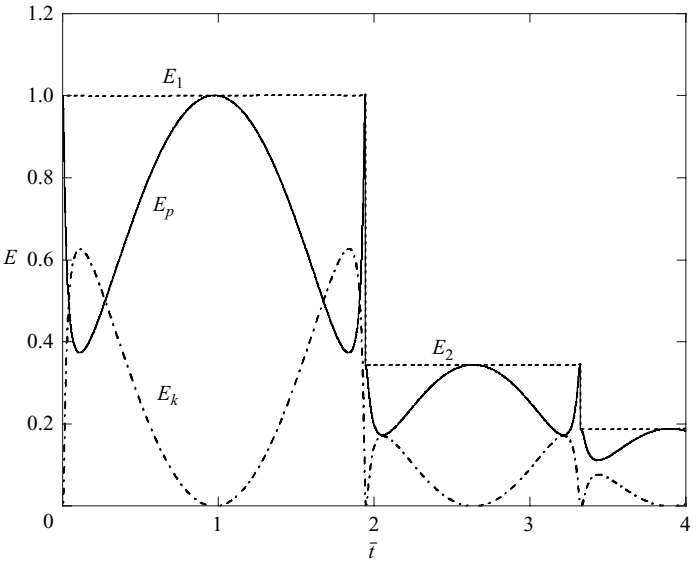

FIGURE 1. Energy balance (the kinetic and potential energies) of the spherical explosion bubble; 0.249 kg tetryl charge at a depth of 91.44 m below the free surface. The energy is normalized with the initial energy E_1. Time is also non-dimensionalized. The parameters for the calculation are $\varepsilon_1 = 103.36$, $\lambda = 1.25$ and $\bar{R}_0 = 0.1467$.

discussion in § 2.1). The zero kinetic energy at the bubble minimum volume allows for a simple implementation of a discontinuous jump condition in the strength parameter. The prediction used the same fraction of total energy, which was estimated from the experiment (see table 1). The incorporation of energy loss allows us to match well with the measured bubble radii and bubble periods up to three oscillation cycles (figure 2). For comparison, the prediction for a perfect oscillating system (no energy loss at each cycle) is also displayed in figure 2.

Some small-scale experiments at the Centre Technique des Systèmes Navals in France in a specially designed test pond have been performed. The pond has a truncated cone shape with a mean radius of 9 m at the top surface, a depth of 7 m and a useful mean radius of 7.5 m at mid-depth. A high-speed camera (1000 images s^{-1}) is used to record the bubble explosion phenomena. The first series of experiments described are the free field explosions. A Hexocire (RDX + wax) charge of 55 g is placed at a depth of 3.5 m. The charge is detonated using an exploding bridgewire detonator (without primary explosive) and a high-energy unit. Further details of the experiments can be found in Klaseboer *et al.* (2005). In figure 3, the selected frames

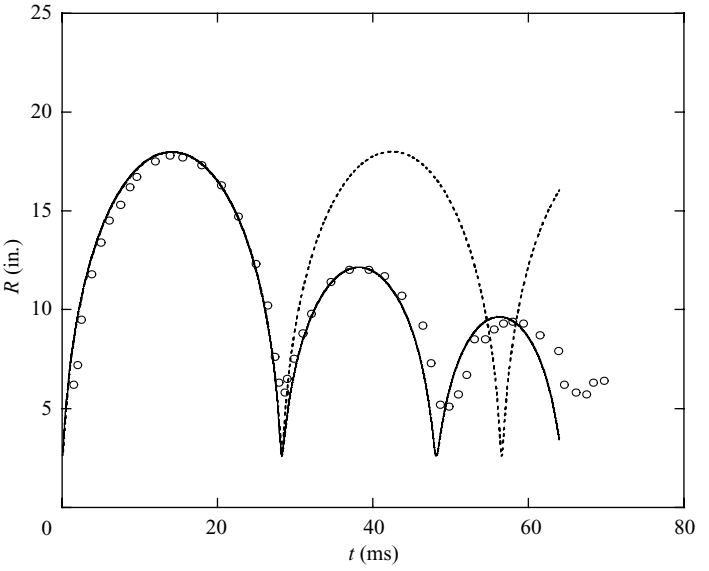

FIGURE 2. Comparison of experimental (circles) and theoretical (solid line) results for radius histories of the spherical explosion bubble, for a 0.249 kg tetryl charge at a depth of 91.44 m below the surface. The theoretical result with no energy loss (dashed line) is also displayed. The experimental data are taken from Cole (1948).

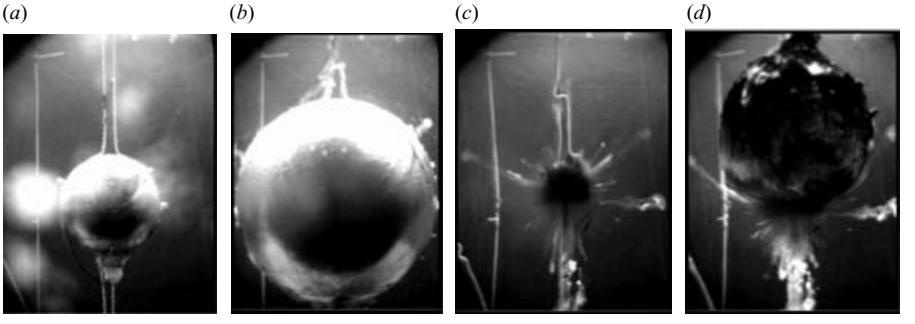

FIGURE 3. Selected frames showing bubble growth, collapse and rebound for a 55 g Hexocire charge at a depth of 3.5 m below the surface. (*a*) $t = 5$ ms, (*b*) $t = 50$ ms (first maximum), (*c*) $t = 94$ ms (first minimum), (*d*) $t = 130$ ms (second maximum), $R_{m,2}/R_{m,1} \approx 0.73$, for the first two expansion periods $T_2/T_1 = 0.72$.

of bubble shape are shown. The first bubble period is around 94 ms. At roughly $t = 50$ ms, the bubble reaches its first maximum size. The ratio of the first two bubble maximum radii ($R_{m,2}/R_{m,1}$) is estimated to be around 0.73. For the bubble period, we merely compared the first two expansion periods ($36/50 = 0.72$). Overall, the two test cases considered here for the explosion-generated bubbles show similar results in terms of the system energy remaining in the second cycle (an energy loss of about 70 % with $E_2/E_1 \sim 0.3$).

3.2. *Cavitation bubble*

A set of carefully controlled experiments were carried out using spark-generated bubbles with a high-speed camera (Buogo & Cannelli 2002). These were done in a laboratory tank 1 m long, 4 m wide and 5.5 m deep, filled with fresh water. The depth

Cycle	First period	Second period
Fraction of available energy remaining (%)	100	24
Fraction of original energy remaining (%)	100	24
R_m (mm)	35.1	21.7
T (ms)	6.3	3.8

TABLE 2. Energy losses in contractions of the spark-generated bubble, maximum bubble radii, and bubble periods from Buogo & Cannelli (2002). $(E_2/E_1)^{1/3} = R_{m,2}/R_{m,1}$ $(= 0.62) \approx T_2/T_1$ $(= 0.60)$ using (3.6).

of the source is 2.5 m and the reference pressure at this depth is $p_\infty = 1.25$ bar. The bubble pulses were measured at a distance of 1.5 m from the source by a hydrophone with normal bandwidth 350 KHz. The vapour bubble generated with a 720 J spark is used for comparison to our model. The maximum bubble radius is 35.1 mm in the first cycle and decreases to 21.7 mm in the second cycle. The bubble periods are 6.3 ms and 3.8 ms, respectively. The experimental data are summarized and analysed in table 2. Again the data correlate reasonably well with (3.6) or with (2.6) and (2.7) if P_v is set to 0. The second bubble period and the bubble maximum radius are around 60 % of the first ones, while those are around 70 % for the previous explosion bubbles. This might suggest that the cavitation bubble loses slightly more energy. This could be cavitation bubbles collapse more violently since less because internal resistance in the form of bubble pressure is available. Correspondingly, the emitted shock waves and corresponding energy losses might be larger.

However, as discussed in § 2, Buogo & Cannelli estimated that the vapour pressure was not negligible in their experiments. It was determined (using the collapse time–maximum radius correlation of (2.8)) to be about $P_v = 0.3$ bar for the first cycle and $P_v = 0.06$ bar for the second cycle. If these values are incorporated into (2.6), $(E_2/E_1)^{1/3} = 0.67$. Based on (2.7), this value becomes slightly larger at $(E_2/E_1)^{1/3} = 0.73$. This would mean an energy loss of about 70 % according to (2.6) and 62 % according to (2.7). These two values are comparable again to those found in § 3.1 for explosion bubbles. To conclude, we can state that the energy loss for a large number of oscillating bubble systems is 60 to 70 % (nearly two-thirds) for each cycle, regardless of their maximum size or origin.

As shown in figure 4, the incorporation of energy loss allows us to match well with the measured bubble radii and bubble periods of Buogo & Cannelli (2002). In this particular simulation, $\Delta P = P_\infty - P_v$ is set to 1.0 bar for both bubble cycles (thus $P_v = 0.25$ bar). The parameters for the calculation of this example are: $\varepsilon_1 = 700$, $\lambda = 1.4$ and $\bar{R}_0 = 0.0844$. The prediction used the same fraction of total energy, which was estimated from the experiment (see table 2).

Figure 5 shows the comparison of continuous pressure–time records measured at a distance of 1.5 m from the source (using (2.10)). The first and second collapse bubble pulses are estimated at 6.3 and 10.4 ms, respectively. Note that several reflection pulses due to the boundary are observed in the experiment.

4. Axisymmetric bubble system

4.1. *Boundary integral method*

Figure 6 shows a schematic view of the problem to be considered in this paper. Again, surface tension and viscous effects are not accounted for in this study. The boundary

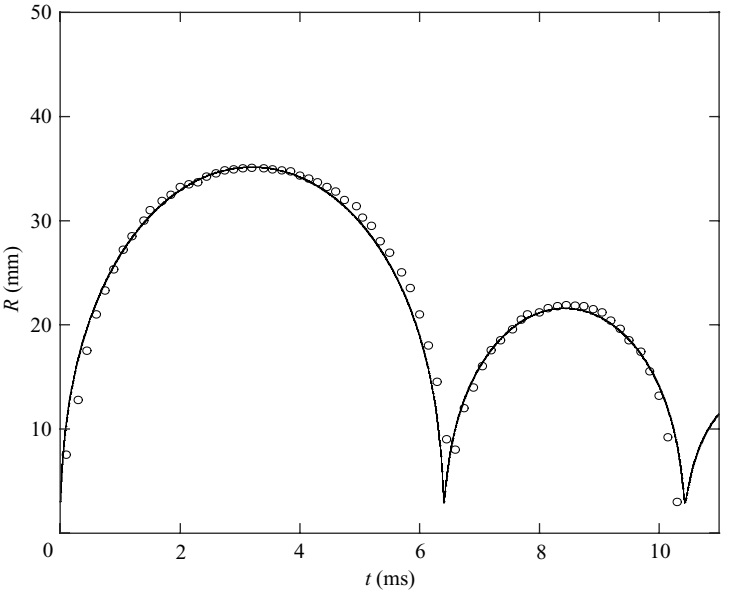

FIGURE 4. Comparison of experimental and simulation results for radius histories of the spark-generated spherical cavitation bubble characterized by $\varepsilon_1 = 700$, $\lambda = 1.4$ and $\bar{R}_0 = 0.0844$; 720 J spark, $R_{m,1} = 35.1$ mm, $R_{m,2} = 21.7$ mm. The experimental data (circles) are from Buogo & Cannelli (2002).

of the bubble is denoted as S, and the fluid domain Ω. The boundary element method takes advantage of Green's theorem, by reducing the Laplace equation to an integral equation. The solution of the Laplace equation on the boundary of the fluid domain, or bubble surface S, is obtained as

$$c(\boldsymbol{P})\,\phi(\boldsymbol{P}) + \int_S \phi(Q)\frac{\partial G(\boldsymbol{P},\,\boldsymbol{Q})}{\partial n}\,\mathrm{d}S = \int_S G(\boldsymbol{P},\,\boldsymbol{Q})\frac{\partial \phi(\boldsymbol{Q})}{\partial n}\,\mathrm{d}S, \tag{4.1}$$

where $c(\boldsymbol{P})$ is the solid angle of a fixed point $\boldsymbol{P}$ on the bubble surface with the integration variable $\boldsymbol{Q}$ also situated on the boundary, and $\boldsymbol{n}$ is taken outward from the liquid into the bubble. Equation (4.1) relates the normal velocity $\partial\phi/\partial n = \boldsymbol{n}\cdot\nabla\phi$ to the potential everywhere on the bubble surface. Note that the integral is carried out only on the bubble surface as the infinite flat rigid-wall effect has been taken into account in the Green function G

$$\mathrm{G}(\boldsymbol{P},Q) = \frac{1}{|\boldsymbol{P}-\boldsymbol{Q}|} + \frac{1}{|\boldsymbol{P}'-\boldsymbol{Q}|}, \tag{4.2}$$

with $\boldsymbol{P}'$ being the reflected image of $\boldsymbol{P}$ with respect to the wall. It is trivial to verify from (4.2) that $\partial G(\boldsymbol{P},\,\boldsymbol{Q})/\partial n = 0$ on the rigid wall. Equation (4.2) is actually the Green function for a three-dimensional configuration, but it is also valid for axial symmetric simulations (but not for truly two-demensional simulations). Strictly (mathematically speaking), $c(\boldsymbol{P})$ is equal to 4π when $\boldsymbol{P}$ is located in the fluid domain, it is 0 when $\boldsymbol{P}$ is located outside the fluid domain and the actual value of $c(\boldsymbol{P})$ is 2π when $\boldsymbol{P}$ is located on a smooth surface S. However, the numerical discretization will lead to slightly non-smooth surfaces and $c(\boldsymbol{P})$ will be close to 2π, but not exactly. If one just takes 2π regardless, it can lead to numerical instabilities. There is, however, an

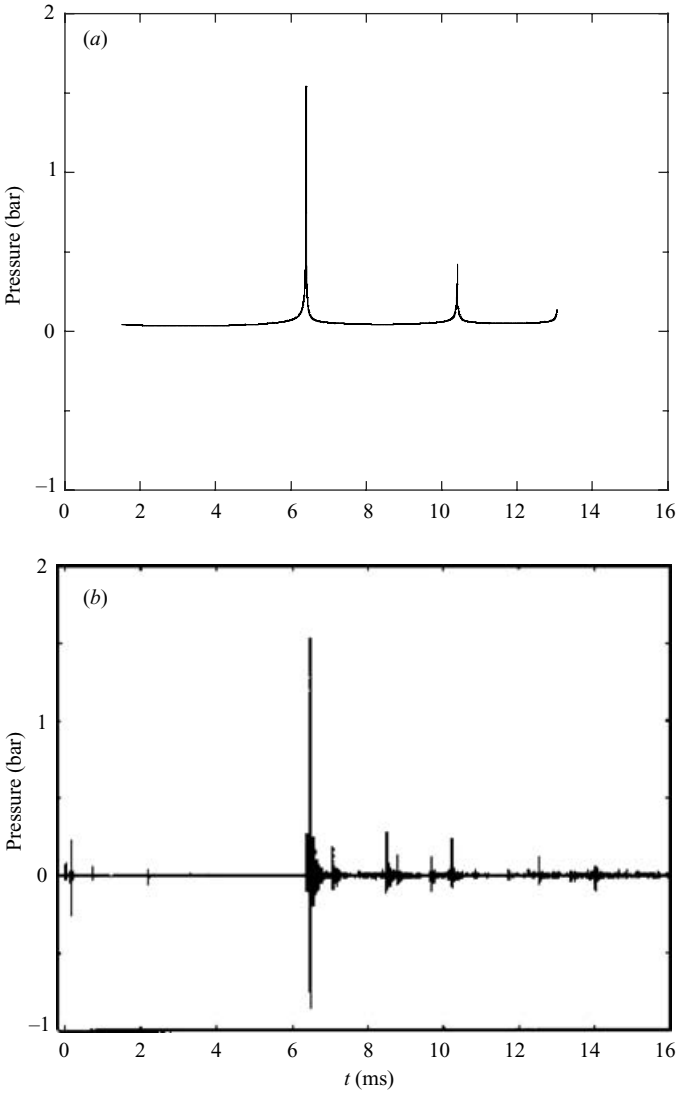

FIGURE 5. Comparison of (*a*) simulation and (*b*) experimental results for pressure waves from the spark-generated spherical cavitation bubble; 720 J spark. The first collapse pulse appears at 6.3 ms, and the second pulse at 10.4 ms. The data are from Buogo & Cannelli (2002).

alternative way for which there is no need to calculate the precise value of $c(\boldsymbol{P})$ (as will be explained later).

Suppose we know the bubble geometry S and the potential on S at some time t. Equation (4.1) is then a Fredholm integral equation of the first kind for the normal fluid velocity at the bubble surface. With the velocity of liquid at the surface of the bubble known, the motion of the interface is determined by

$$\frac{\mathrm{D}\boldsymbol{X}}{\mathrm{D}t} = \nabla\phi, \tag{4.3}$$

where $\boldsymbol{X}$ is the position vector and described in the Lagrangian sense: $\mathrm{D}/\mathrm{D}t = \partial/\partial t + u \cdot \nabla$. The time evolution of the velocity potential is obtained by the unsteady

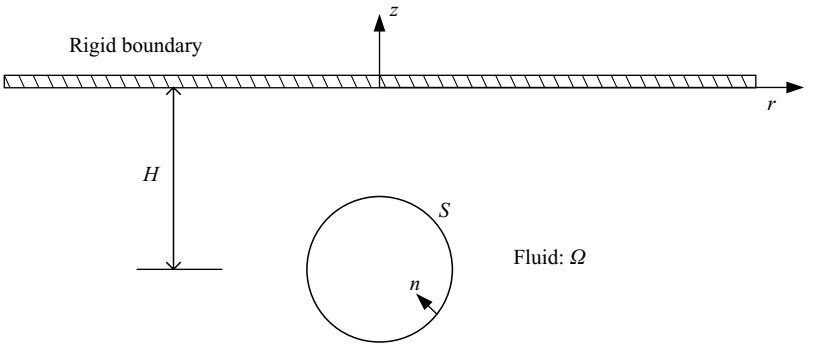

FIGURE 6. The geometry used to consider axisymmetric bubble motion near a wall.

Bernoulli's equation valid on the bubble surface as (dimensionless)

$$\frac{\mathrm{D}\bar{\phi}}{\mathrm{D}\bar{t}} = 1 + \tfrac{1}{2}|\nabla\bar{\phi}|^2 - \varepsilon(\bar{V}_0/\bar{V})^{\lambda}, \tag{4.4}$$

Again, gravity is neglected in (4.4), but could easily be included by adding a term $(-\delta^2\bar{z})$ to the right-hand side of this equation, where the vertical coordinate z on the bubble surface must be used and the previously introduced buoyancy parameter δ. A variable time stepping scheme is used (Best & Kucera 1992)

$$\overline{\delta t} = \frac{\overline{\Delta\phi}}{\max\left(\tfrac{1}{2}|\nabla\bar{\phi}|^2 + \varepsilon(\bar{V}_o/\bar{V})^{\lambda} + 1\right)}, \tag{4.5}$$

where $\Delta\bar{\phi}$ was chosen to be 0.02 in most of the computations.

The numerical method works as follows. Determine the time step with (4.5), and next update the potential on the bubble surface with (4.4). Now (4.1) can be used to set up a system of equations relating the known potential and the unknown normal velocities. One of the difficulties related to boundary element methods is the treatment of the singularities when $\boldsymbol{Q}$ approaches $\boldsymbol{P}$ in (4.1). The inverse potential problem (thus inside the bubble) can give an expression for the diagonal term of the matrix with the potential term (the discretized version of the whole left-hand side of (4.1) which also contains the strongest singularities). It appears that the diagonal terms of the matrix are just 4π minus the sum of all the other elements in the same row (the so-called 4π rule). More details can be found in Liu & Rudolphi (1999). Moreover, this treatment makes it redundant to calculate the exact value of $c(P)$ in (4.1). The weaker singularity found on the right-hand side of (4.1) (the term with the normal velocities) can be eliminated using an analytical expression. The normal velocities can be solved from the resulting matrix equation. The tangential velocity at the bubble surface can be obtained with the help of the potential distribution at this surface. Once the normal and tangential velocities are known, the velocity vector $u = \nabla\phi$ can be constructed. The position of the bubble surface can be updated with (4.3). A new volume of the bubble will give rise to a new gas pressure (last term in (4.4)). Now all variables are known and we can then proceed with the next time step. More on the numerical details can be found in Wang *et al.* (1996).

4.2. *Modification for toroidal geometry and rejoining*

During the collapse phase of the bubble, usually a liquid jet is created that traverses across the bubble with very high speed. If the liquid jet impacts on the opposite

face of the bubble, the fluid domain becomes doubly connected. Numerically, two challenges arise when this happens. First of all, some re-meshing has to be performed in order to connect the fluid of the jet and the fluid on the far side of the bubble. In an axial symmetrical configuration this is quite straightforward (Pearson *et al.* 2004 or Wang *et al.* 1996). Furthermore, the jet impact will generate a circulation in the fluid. Zhang & Duncan (1994) have modelled this circulation by introducing a vortex sheet that moves with the fluid. This vortex sheet can become highly distorted as the bubble evolves. A simpler model consists of placing a vortex ring inside the bubble enclosing the jet. The strength of this vortex ring is chosen to be equal to the potential difference of the jet tip and the opposite bubble surface just before the jet impacts. The potential is now decomposed into two parts, one corresponding to the circulation of the jet impact (Ψ) and a remainder (φ)

$$\phi = \Psi + \varphi. \tag{4.6}$$

The potential Ψ exhibits a jump across the vortex ring; the potential φ is smooth throughout the whole fluid domain. An analytical solution can be found for the velocity field generated by Ψ. See Wang *et al.* (1996) for more details.

As the toroidal bubble is re-expanding, the jet will weaken and the jet area will also become smaller and smaller. Best (1994) took this effect into account by letting the bubble rejoin on the axis of symmetry. In our numerical simulations, the bubble is assumed to rejoin when a node on the bubble has reached a dimensionless radius of less than 0.01. This value has been chosen also in order to prevent numerical instabilities which can occur at lower values. The recommended value is between 0.01 and 0.05. A doubly connected bubble is now transformed into a singly connected one. In order for this to happen, the node that has reached the said value of 0.01 and its neighbour that is nearest to the axis of symmetry (either the node above or below it) are placed on the axis of symmetry. It is reckoned that the total potential remains constant at these two nodes for such small displacements. In fact, in the rejoining process, the opposite procedure from the jet impact procedure is followed. The vortex ring is taken out again. Its potential is added to the total potential according to (4.6). From now onwards, the boundary integral equations are applied identically as was done before the jet impact. Two simple tests were performed to ensure that the procedure followed is correct. First, the energy levels before and after rejoining are checked and remain constant. Secondly, the velocity profiles for all nodes just before and just after the rejoining procedure are compared with each other and show no noticeable differences.

4.3. *Some results*

4.3.1. *Verification with the spherical bubble*

In order to verify the axisymmetric code, the previous spherical case for an explosion bubble was simulated. The asymmetry in the flow field is due to the presence of the boundary. For motion near a boundary it is necessary at this time to introduce a dimensionless stand-off parameter γ as

$$\gamma = H/R_{m,1}, \tag{4.7}$$

where H is the distance away from the boundary at which inception of the bubble occurs. Setting $\gamma > 20$ in the calculation, the influence of the wall becomes negligible and a spherical symmetrically oscillating bubble should be obtained. As shown in figure 7, the prediction using the axisyimmetric code corresponds very well to the

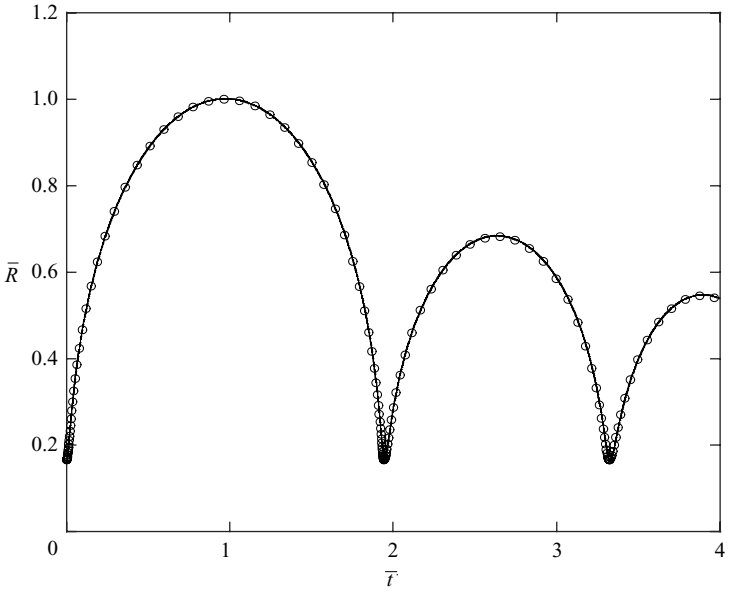

FIGURE 7. Comparison for radius histories of the spherical explosion bubble using the Rayleigh–Plesset equation (solid line) and the axisymmetric simulation code (circle), for the same case as figure 2 (results are non-dimensionalized).

theoretical prediction obtained by the Rayleigh–Plesset equation for the previous explosion bubble case of § 3.1 (variables are plotted dimensionless now).

4.3.2. *A system with no energy loss*

Consider an oscillating bubble as a system with no energy loss. A typical example of bubble motion ($\lambda = 1.4$) can be taken for $\gamma = 2.0$ and the strength parameter $\varepsilon = 100$ with the corresponding initial radius equal to $\bar{R}_0 = 0.1651$. Figure 8 shows the evolution of the bubble for the first expansion and collapse period. When the bubble reaches its maximum size, it is still kept nearly spherical. In the consequent collapsing phase, the high-speed liquid jet is formed. It eventually impacts on the other side of the bubble at non-dimensional time of $\bar{t} = 2.1085$, and a doubly connected toroidal geometry is formed via the employment of a vortex ring. Figure 9 shows the further evolution of the toroidal bubble which is in the process of rebounding. The minimum volume occurs at this toroidal stage (figure 9*b*). This example is as that shown in Best (1993) and the shapes are very similar.

The further evolutions of the bubble for the second expansion and collapse period are shown in figure 10. The remarkable feature is that the bubble resumes the singly connected geometry in the rebounding period, and that it starts to form a second liquid jet in the re-collapsing period. This demonstrates a scenario for a perfect oscillating system (no energy loss).

In order to gain more insight into the oscillating bubble system, the energy balance (and its components) is shown in figure 11. It can be observed that the total energy is maintained throughout, although there seem to be some accumulated numerical errors in the late stage of the second bubble period. The first minimum in kinetic energy corresponding to the first maximum bubble volume at around $\bar{t} = 1$ is virtually zero, which is strictly true only for a spherical bubble system. As shown in the figure

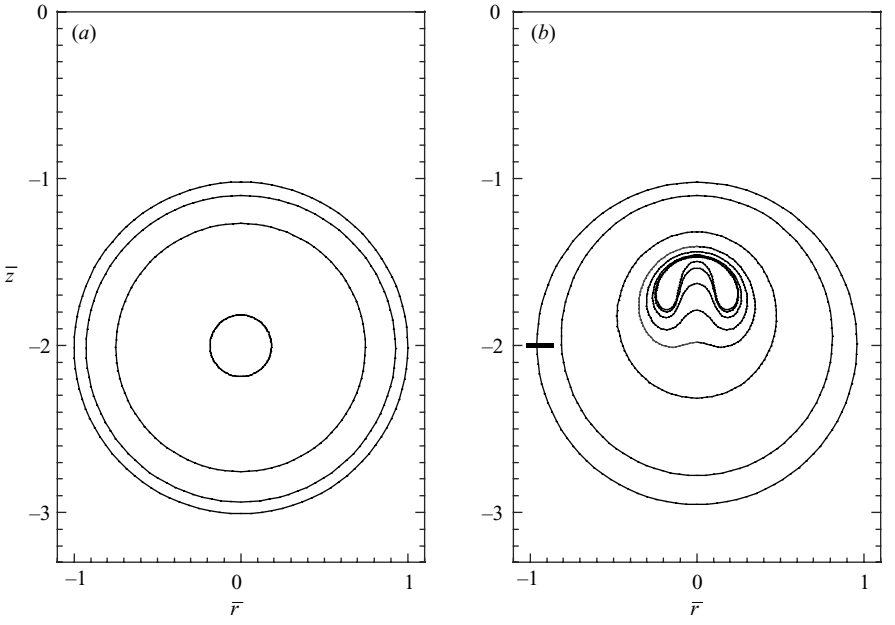

FIGURE 8. The expansion and collapse of a bubble characterized by $\gamma = 2.0$ and $\varepsilon = 100$. Dimensionless times corresponding to successive profiles are: (*a*) expansion phase: 0.0089, 0.3169, 0.6233, 0.9906; (*b*) collapse phase: 1.3674 (outermost), 1.6907, 2.0003, 2.0645, 2.0824, 2.1075 and 2.1040 (innermost). The marks on the left-hand side of the figure indicate the horizontal position of the bubble creation location (results are non-dimensionalized).

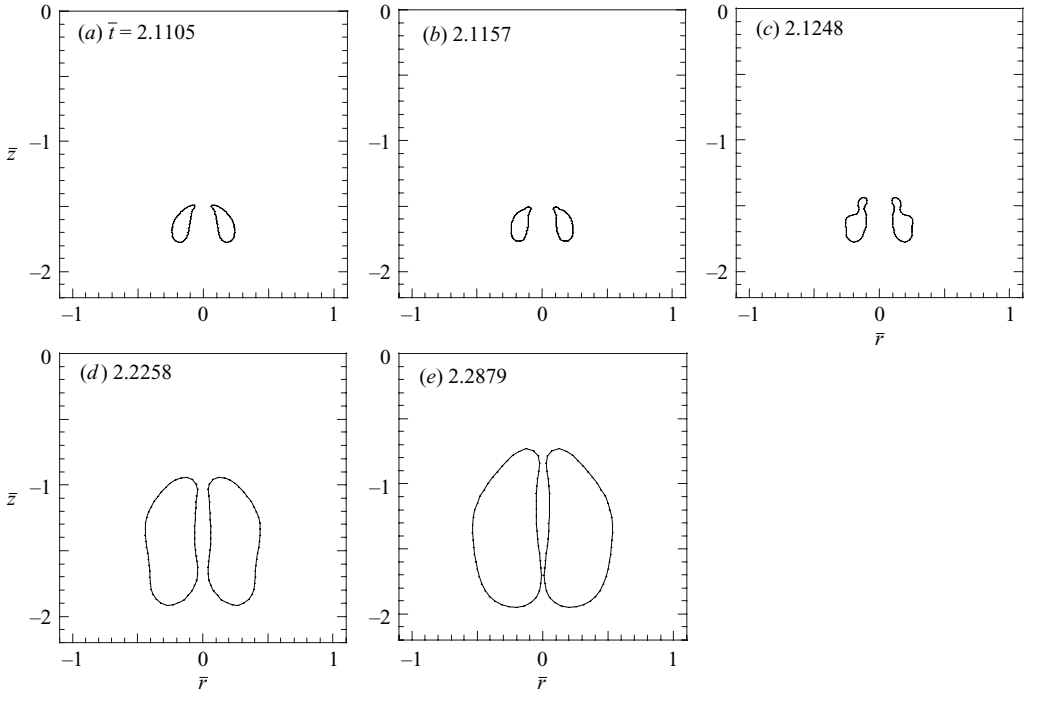

FIGURE 9. The motion of the toroidal bubble (non-dimensionalized) that evolves from the collapse of a bubble characterized by $\gamma = 2.0$ and $\varepsilon_1 = \varepsilon_2 = 100$. Minimum bubble volume is shown in (*b*). Note that no energy loss is considered in the rebounding phase.

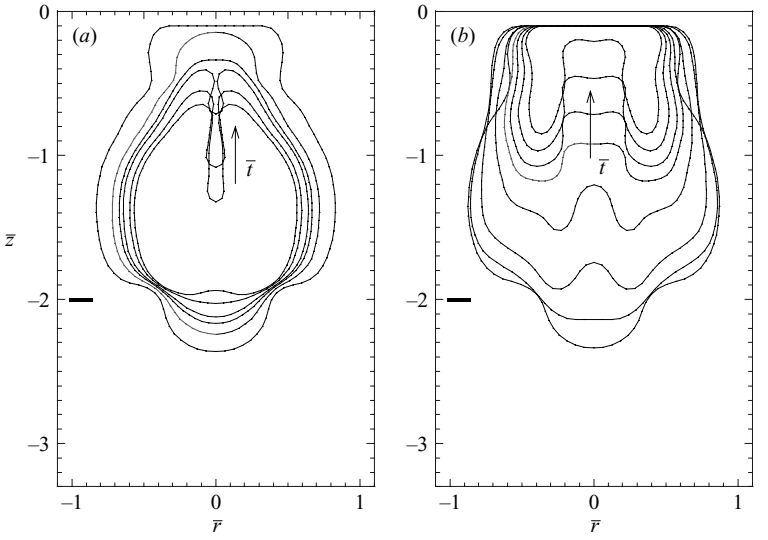

FIGURE 10. The dimensionless rebounding and re-collapse of a bubble characterized by $\gamma = 2.0$ and $\varepsilon_1 = \varepsilon_2 = 100$. Dimensionless times are: (*a*) rebounding phase: $\bar{t} = 2.3151$ (innermost), 2.3457, 2.3966, 2.4299, 2.5046, 2.7651 (outermost); (*b*) re-collapse phase: 3.1111 (outermost), 3.5699, 3.7356, 3.9697, 4.0946, 4.1511, 4.2105 and 4.2697 (innermost). The marks on the left-hand side of the figure indicate the horizontal position of the bubble creation location.

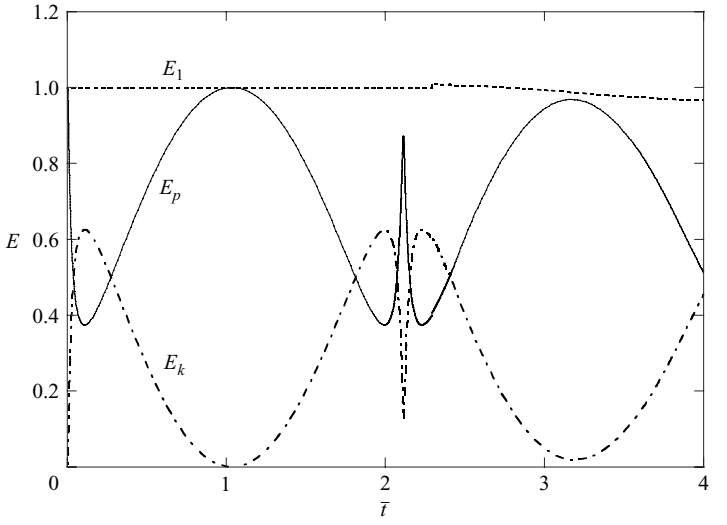

FIGURE 11. Normalized energy balance of a bubble system characterized by $\gamma = 2.0$ and $\varepsilon_1 = \varepsilon_2 = 100$, as shown in figures 8, 9 and 10. Note that the kinetic energy at minimum volume is no longer zero, indicating some part of the bubble being in motion (toroidal bubble). The total energy (= 4.7302) is maintained up to the second oscillation period (time is dimensionless).

at around $\bar{t} = 2$, the second minimum corresponding to the first minimum volume occurs at the toroidal stage. Here, we note the kinetic energy is no longer zero, indicating that some parts of the bubble are still in motion (Pearson *et al.* 2004).

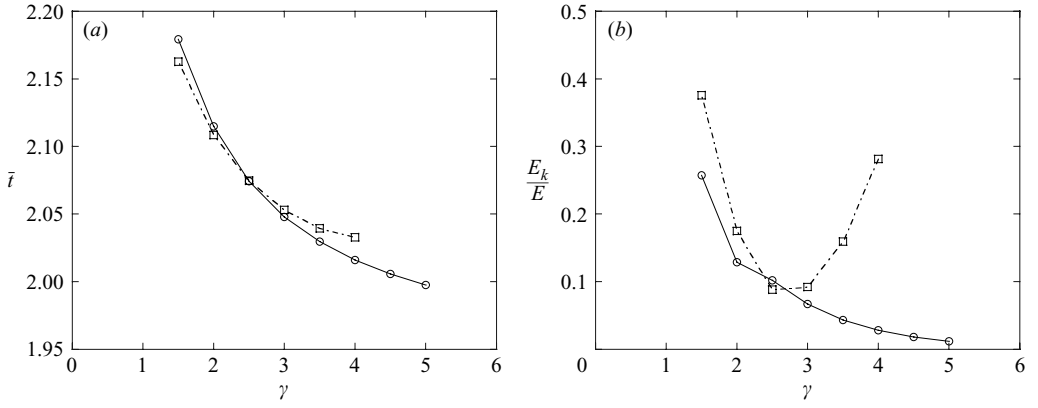

FIGURE 12. Some data for the toroidal stage over a range of standoff distances γ. (*a*) The dimensionless times of jet impact (square) and bubble minimum volume (circle); (*b*) kinetic energies at those times as a percentage of the total energy.

4.3.3. *The minimum volume stage*

Before we discuss our calculations for the more realistic system with energy loss, it is instructive to examine the minimum volume stage (in which the loss of energy will be incorporated) in terms of the magnitude of kinetic energy and bubble topology. Figure 12(*a*) shows the variations of times of bubble minimum volume and formation of toroidal bubble as a function of γ. For a distance of $\gamma < 2.5$, the toroidal bubbles form before they reach a minimum volume. This is due to the strong asymmetric force caused by the boundary. For $2.5 < \gamma < 4.0$, the bubble minimum volume occurs before the formation of the toroidal shaped bubble. That is, the bubble can evolve into a toroidal form even in the rebounding phase owing to the high inertia of the jet. For larger distances, however, the jet cannot completely penetrate the bubble during the non-spherical rebounding phase (no toroidal geometry). Eventually, the oscillating system behaves almost spherically for $\gamma > 10$. Figure 12(*b*) shows the calculated kinetic energy at the time of jet impact and at the time of bubble minimum volume as a function of γ. We note the ratio of the kinetic energy to total energy at bubble minimum volume decreases and becomes virtually zero for $\gamma = 10$. On the other hand, the kinetic energy estimated at the time of toroidal formation reaches a minimum value at a distance of $\gamma \approx 2.5$ and starts to increase up to $\gamma = 4$ (no toroidal shaped bubble is formed above this value).

4.3.4. *A system with energy loss*

In this section, we consider an oscillating bubble system with some energy loss. All parameters are set equal to the previous example of a bubble motion ($\gamma = 2.0$ and $\varepsilon_1 = 100$, $\lambda = 1.4$), except that the strength parameter is discontinuously replaced by a new value ε_n, to reduce the potential energies at each bubble volume minima. Figure 13 shows an example of the energy balance for $\varepsilon_2 = 80$. As seen, the total energy in the system undergoing several cycles is maintained only for each oscillation period. Note that the total energy in the second cycle is not exactly 80 % of that of the first cycle. This is because the kinetic energy at bubble minimum volume is not zero, and only the potential energy estimated at that time is reduced by 20 %.

Figure 14 shows the kinetic energies calculated from the time of minimum volume until the time of resumption of a singly connected bubble topology in the rebounding

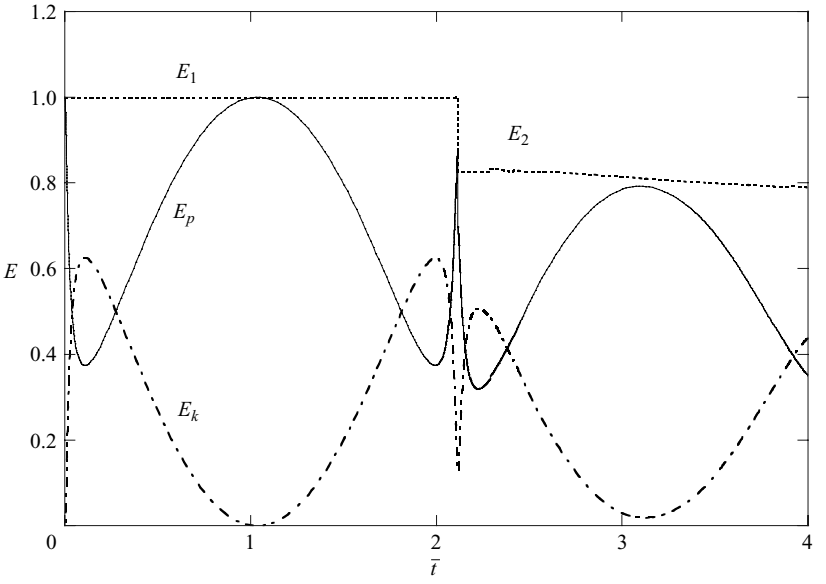

FIGURE 13. An example of (normalized) energy balance up to the second oscillation period with a consideration of some energy loss. The potential energy estimated at the bubble minimum volume is reduced by 20 %. The total energy in the second cycle is not 80 % of that of the first cycle owing to the non-zero kinetic energy. There is some numerical error accumulation at the late stage of the second cycle. Time is made dimensionless.

phase for a range of ε_2 values. In figure 14(*a*) the values for $\gamma = 2$ are shown and in figure 14(*b*) for $\gamma = 3$. The results until the time of bubble minimum volume are the same, so they are not shown here. The extent of rapid energy deposition from potential energy to kinetic energy during the early rebounding phase varies with the amount of energy reduction in the system. We note that the toroidal bubble for $\gamma = 3$ evolves into a singly connected bubble faster than that for $\gamma = 2.0$ ($\bar{t} = 2.06$ *vs.* $\bar{t} = 2.12$, respectively). In general, the kinetic energy within the doubly connected bubble can reach up to 63 % of the system total energy.

Figure 15 shows the evolution of the previous bubble for the rebound and re-collapse period (see figure 10), but with a reduced value of $\varepsilon_2 = 30$. Note that the rigid boundary is located at $z = 0$ in this figure. The rejoining starts in the part of the bubble nearest to the wall and starts to close like a zipper away from the wall during the re-expansion stage. The second period is much shorter than the previous no-energy-loss case. This is also consistent with the spherical oscillating bubble system described previously.

One remarkable difference compared with the previous case of a perfect system is that a counterjet develops very rapidly in the rebounding stage with a combination of the necking process. In the following re-collapsing period, it starts to collapse and eventually a second jet evolves. Vogel *et al.* (1989) have shown that a counterjet develops only for $\gamma > 1$. Lindau & Lauterborn (2003) confirmed this and found that no counterjet develops above $\gamma \approx 3$. For a high value of γ, he jet impact does not happen, and no counterjet arises. For $\gamma < 1$, the bubble directly impacts on the wall during expansion, resulting in no counterjet. Hence, the counterjet is coupled with an impact of the jet on the other bubble surface. Another mechanism contributing to the development of the counterjet can be attributed to cavitation inception which follows

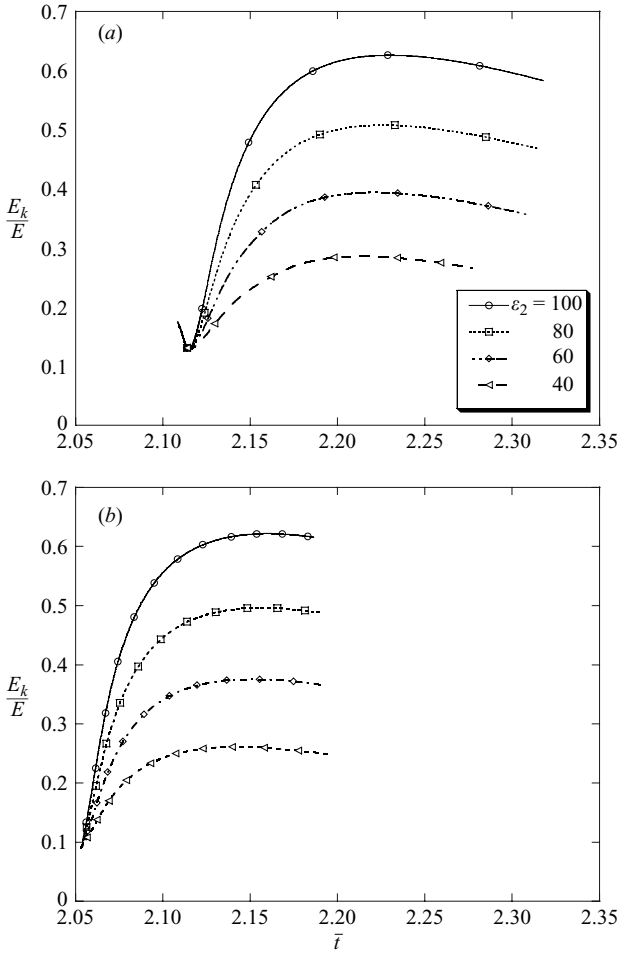

FIGURE 14. The variations of kinetic energy for the toroidal stage (from jet impact up until the time of rejoining into a singly connected shape) for a range of gas pressures ε_2. (*a*) $\gamma = 2.0$, (*b*) $\gamma = 3.0$. Time is made dimensionless.

the propagation of the 'jet torus shock wave', which is the energy loss mechanism. Some discussions about the creation mechanisms of the counterjet were given by Lindau & Lauterborn (2003).

The couterjet has been observed only in the experiments (see e.g. Tomita & Shima 1986; Vogel *et al.* 1989; Ward & Emmony 1991; Philipp & Lauterborn 1998; Kodama & Tomita 2000), and has never been captured in fluid dynamic simulations (Lindau & Lauterborn 2003). In fact, the simulations are, in principle, not realistic without any incorporation of energy loss into the oscillating system. Some experimental pictures (Lindau & Lauterborn 2003) are shown in figure 16 and the shapes are very similar to the present prediction. Note that the rigid boundary is below in this figure and the main body of the bubble is not shown. The horizontal location of the counterjet tip is near the bubble creation location, which is also estimated in the simulation of figure 15. Because of fluid instabilities on the bubble interface some parts of the counterjet may remain in the system as shown in figure 16. These instabilities are not covered by the present numerical scheme.

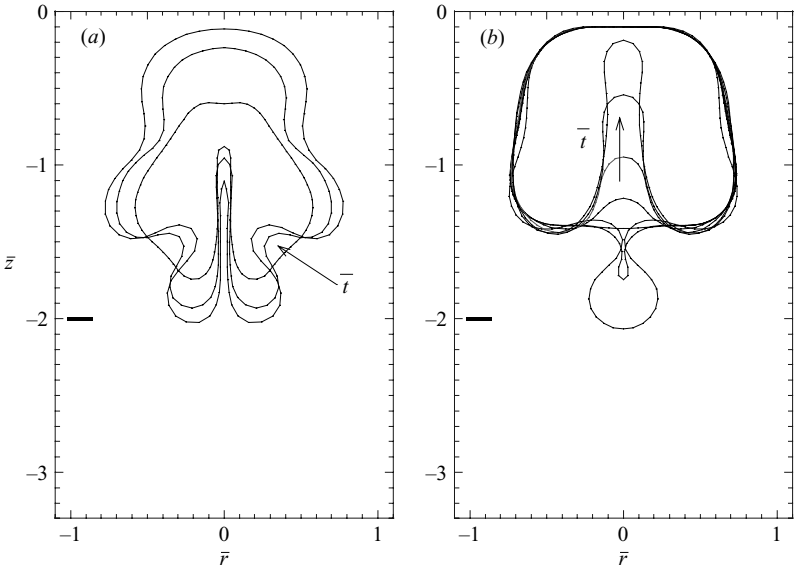

FIGURE 15. The dimensionless rebounding and re-collapse of a bubble characterized by $\gamma = 2.0$, $\delta = 0$, $\varepsilon_1 = 100$ and $\varepsilon_2 = 30$. Dimensionless times are: (*a*) rebounding phase: $\bar{t} = 2.3647$ (innermost), 2.5253, 2.7568 (outermost); (*b*) re-collapse phase: 2.9903, 2.9959, 2.9975, 3.0050, 3.0210, 3.0552 and 3.0980. The second period is shorter than the previous case with no energy loss (see figure 10). The marks on the left-hand side of the figure indicate the horizontal position of the bubble creation location.

FIGURE 16. Onset of the counterjet for $\gamma = 2.6$, 2.2 and 1.8 (top to bottom), 10, 120, 250, 500, 1000, 2000, 4000 and 8000 ns after shock wave emission. $R_m = 1.5$ mm, frame width 0.97 mm. Note that the rigid boundary is below. The marks on the left-hand side of the figure indicate the horizontal position of the bubble creation location (reproduced with permission from Lindau & Lauterborn 2003).

5. Conclusions

The boundary integral method has been widely applied to the analysis of cavitation (or explosion) bubbles only up to toroidal bubbles that occur during collapse in the neighbourhood of a boundary. In this paper, the further evolution (rebound) of the toroidal bubble is considered with energy loss in the system taken into account. The energy loss in the oscillating bubble system is incorporated into the mathematical model by a discontinuous jump in the potential energy at the minimum volume during the short collapse–rebound period accompanying wave emission.

The first part of this study is the evaluation of the spherically symmetric motion of a bubble using the Rayleigh–Plesset equation with the system energy loss taken into account. Excellent agreement with experimental data for the bubble radius evolution

up to three oscillation periods is obtained, indicating the suitability of the current implementation. For the tested explosion-generated and spark-generated bubbles, the total energy in the second cycle is around 30 % of that in the first cycle.

Next, the loss of system energy is incorporated into the boundary integral method for the analysis of rebounding bubbles in the neighbourhood of a rigid boundary, in an asymmetric geometry. By taking the system energy loss into account, the peculiar entity, counterjet, which has never been captured in the simulations, seems to appear during the rebounding phase.

The authors would like to thank Professor Werner Lauterborn for allowing reproduction of figure 16. This work was carried out during the visit of M. L. to the National University of Singapore. M. L. acknowledges the financial support by the Korea Research Foundation Grant (KRF-2004-013-D00058).

REFERENCES

Benjamin, T. B. & Ellis, A. T. 1966 The collapse of cavitation bubbles and the pressures thereby produced against solid boundaries. *Phil. Trans. R. Soc. Lond.* A **260**, 221–240.

Best, J. P. 1993 A The formation of toroidal bubbles upon the collapse of transient cavities. *J. Fluid Mech.* **251**, 79–107.

Best, J. P. 1994 The rebound of toroidal bubbles. In *Bubble Dynamics and Interface Phenomena* (ed. J. R. Blake, J. M. Boulton-Stone & N. H. Thomas), pp. 405–412. Kluwer.

Best, J. P. & Kucera, A. 1992 A numerical investigation of non-spherical rebounding bubbles. *J. Fluid Mech.* **245**, 137–154.

Blake, J. R., Taib, B. B. & Doherty, G. 1986 Transient cavities near boundaries. Part 1. Rigid boundary. *J. Fluid Mech.* **170**, 479–497.

Boulton-Stone, J. M. 1993 A comparison of boundary integral methods for studying the motion of a two-dimensional bubble in an infinite fluid. *Comput. Methods Appl. Mech. Engng* **102**, 213–234.

Brennen, C. E. 1995 *Cavitation and Dubble Dynamics*, Oxford University Press (available online).

Brujan, E. A., Keen, G. S., Vogel, A. & Blake, J. R. 2002 The final stage of the collapse of a cavitation bubble close to a rigid boundary. *Phys. Fluids* **14**, 85–92.

Buogo, S. & Cannelli, G. B. 2002 Implosion of an underwater spark-generated bubble and acoustic energy evaluation using the Rayleigh model. *J. Acoust. Soc. Am.* **111**, 2594–2600.

Chahine, G. L. & Perdue, T. O. 1988 Simulation of the three-dimensional behaviour of an unsteady large bubble near a structure. In *Proc. 3rd Intl Colloq. on Drops and Bubbles, Monterey, CA.*

Cole, R. H. 1948 *Underwater Explosions*. Princeton University Press.

Delale, C. F. & Tunç, M. 2004 A bubble fission model for collapsing cavitation bubbles. *Phys. Fluids* **16** (11), 4200–4203.

Geers, T. L. & Hunter, K. S. 2002 An integrated wave-effects model for an underwater explosion bubble. *J. Acoust. Soc. Am.* **111**, 1584–1601.

Klaseboer, E., Hung, K. C., Wang, C., Wang, C. W., Khoo, B. C., Boyce, P., Debono, S. & Charlier, H. 2005 Experimental and numerical investigation of the dynamics of an underwater explosion bubble near a resilient/ rigid structure. *J. Fluid Mech.* **537**, 387–413.

Kodama, T. & Tomita, Y. 2000 Cavitation bubble behaviour and bubble-shock wave interaction near a gelatine surface as a study of in vivo bubble dynamics. *Appl. Phys.* B **70**, 139–149.

Lauterborn, W. 1972 High-speed photography of laser-induced breakdown in liquids. *Appl. Phys. Lett.* **21**, 27–29.

Leighton, T. G. 1994 *The Acoustic Bubble*. Academic.

Lew, K. S. F., Klaseboer, E. & Khoo, B. C. 2006 A collapsing bubble-induced micropump: an experimental study. *Sensors Actuators* A (in press).

Lindau, O. & Lauterborn, W. 2003 Cinematographic observation of the collapse and rebound of a laser-produced cavitation bubble near a wall. *J. Fluid Mech.* **479**, 327–348.

Liu, Y. J. & Rudolphi, T. J. 1999 New identities for fundamental solutions and their applications to non-singular boundary element formulations. *Comput. Mech.* **24**, 286–292.

Lundgren, T. S. & Mansour, N. N. 1991 Vortex ring bubbles. *J. Fluid Mech.* **224**, 177–196.

Pearson, A., Blake, J. R. & Otto, S. R. 2004 Jets in bubbles. *J. Engng Maths* **48**, 391–412.

Philipp, A. & Lauterborn, W. 1998 Cavitation erosion by single laser-produced bubbles. *J. Fluid Mech.* **361**, 75–116.

Putterman, S. J. & Weninger, K. R. 2000 Sonoluminescence: how bubbles turn sound into light. *Annu. Rev. Fluid Mech.* **32**, 445–476.

Rayleigh, Lord 1917 On the pressure developed in a liquid during the collapse of a spherical cavity. *Phil. Mag.* **34**, 94–98.

Taylor, G. I. 1942 Vertical motion of a spherical bubble and the pressure surrounding it. In *Underwater Explosion Research,* **2**, 131–144, Office of Naval Research, Washington, DC.

Taylor, G. I. & Davies, R. M. 1944 *UNDEX Rep. 88 UK*.

Tomita, Y. & Shima, A. 1986 Mechanisms of impulsive pressure generation and damage pit formation by bubble collapse. *J. Fluid Mech.* **169**, 535–564.

Vogel, A., Lauterborn, W. & Timm, R. 1989 Optical and acoustic investigations of the dynamics of laser-produced cavitation bubbles near a solid boundary. *J. Fluid Mech.* **206**, 299–338.

Wang, C. & Khoo, B. C. 2004 An indirect boundary element method for three-dimensional explosion bubbles. *J. Comput. Phys.* **194**, 451–480.

Wang, Q. X., Yeo, K. S., Khoo, B. C. & Lam, K. Y. 1996 Nonlinear interaction between gas bubble and free surface. *Comput. Fluids* **25**, 607–628.

Ward, B. & Emmony, D. C. 1991 Interferometric studies of the pressure developed in a liquid during infrared-laser-induced cavitation bubble oscillation. *Infrared Phys.* **32**, 489–515.

Zhang, S. G. & Duncan, J. H. 1994 On the non-spherical collapse and rebound of a cavitation bubble. *Phys. Fluids* **6** (7), 2352–2362.